International Journal of Greenhouse Gas Control, Volume 118, July 2022, Article number 103674
DOI:10.1016/j.ijggc.2022.103674

Real-scale investigation of liquid CO_2 discharge from the emergency release coupler of a marine loading arm

Hisham Al Baroudi[1], Ryota Wada[2]*, Masahiko Ozaki[2], Kumar Patchigolla[1], Makoto Iwatomi[3], Kengi Murayama[3], Toru Otaki[3]

1. Centre for Thermal Energy and Materials (CTEM), School of Water, Energy and Environment (SWEE), Cranfield University, Cranfield, Bedfordshire, MK43 0AL, U.K.

2. Dept. of Ocean Technology, Policy, and Environment, Graduate School of Frontier Sciences, The University of Tokyo, Kashiwa, 277-8561, JAPAN.

3. Nagaoka Works, Tokyo Boeki Engineering Ltd., Nagaoka, 940-0021, JAPAN.

**Corresponding author e-mail: r_wada@k.u-tokyo.ac.jp*

Abstract

Carbon capture, utilisation and storage has been recognised as a necessary measure to reduce greenhouse gas emissions. CO_2 shipping represents a promising transportation option that offers flexible sink-source matching to enable decarbonisation at a global scale. In order to implement safe and reliable loading and offloading operations at the terminal, marine loading arms require the integration of emergency release systems in the event of sudden movement of the ship away from the berthing line. In this study, a cryogenic test facility was constructed to handle CO_2 in proximity of the triple point (~0.9 MPa[abs] – 1.7 MPa[abs], 227 K - 239 K) and replicate the principles of an emergency release coupler during a shutdown, with the aim of investigating the CO_2 discharge and dispersion behaviour. Findings show that separation of the test vessel leads to an abrupt discharge of the liquefied CO_2 inventory and several phase transitions within 0.6 s of the start of the discharge in all tests. The clouds disperse in a 'tulip' shape that could be clearly observed from afar, and generation of carbon dioxide solids was observed on the vessel surface in all performed tests, bringing the temperature inside the vessel to approximately 190 K. The implementation of protective barriers is expected to reduce the impact of the release, though the risk of asphyxiation or cryogenic burns to surrounding personnel cannot be ruled out given the magnitude of the discharge process.

Keywords

GHG; Carbon Capture, Utilisation and Storage; CO_2 transport; CO_2 shipping; marine loading arm, emergency release system

1 Introduction

Transportation of CO_2 by ship allows a flexible sink-source matching in the CCUS chain, and it is particularly indicated when implementation of pipeline systems is unfeasible or impractical (Ozaki et al., 2016, ZEP, 2018; Al Baroudi et al., 2021a). In these regards, potential CO_2 liquid conditions related to shipping transport are conventionally categorised into low pressure conditions (0.6–1 MPa , hereinafter, MPa means MPa[abs]), 218–233 K), medium pressure conditions (1.5–1.9 MPa, 243–253 K) and high pressure conditions (>1.9 MPa and 253 K) (Al Baroudi et al., 2021a, Element Energy, 2018, Ministry of Petroleum and Energy Norway, 2016). Literature indicates low pressure conditions to be optimal, (Huh et al., 2013; Yoo et al., 2013; Skagestad et al., 2014; Mitsubishi Heavy Industries, 2004; Jakobsen et al., 2017) attributing this choice to the lower capital expenditure of the vessels and enhanced cargo density under these conditions. It should be noted that handling carbon dioxide at low pressure conditions is a novel concept that requires development of adequate safety protocols to mitigate the risk of operational challenges during operations (Noh et al., 2018, Al Baroudi et al., 2021a, Brown et al., 2017). Shipping CO_2 at higher liquid pressures (~1.5 MPa) (Ministry of Petroleum and Energy Norway et al., 2016; Seo et al., 2016, IEAGHG, 2020, Al Baroudi et al., 2021a), represents a technologically mature concept characterised by higher capital expenditure and lower operational costs (Seo et al., 2016). With regards to process and operational safety, the UK's Health and Safety Executive highlighted several gaps related to emergency response, temporary refuge, integrity issues and predictions of dry-ice formation (Koers, 2011; Harper et al., 2015) during large-scale releases of dense phase CO_2 in the CCUS chain. During accidental or planned depressurisation of liquid CO_2 in the system, the fluid transitions from its initial liquid or two-phase liquid-vapour envelope to a solid, liquid and vapour three-phase stage when depressurising below the triple point (0.51 MPa, 217 K) as shown in Fig. 1 (Holt et al., 2012). As the fluid's expansion continues to atmospheric pressure, temperatures in the system may reach values around 195 K, and a variable amount of solid phase CO_2 generates in the process depending on initial discharge conditions. Solid CO_2 generating within the system may lead to blockages, therefore creating a significant hazard. Several studies have focused on accidental leakage behaviour of CO_2 typical of pipeline transport, including lab-scale (Pursell, 2012; Li et al., 2015; Xie et al., 2014; Zhou et al., 2014; Teng et al., 2016;

Guo et al., 2017; Wang et al., 2019) and large-scale experiments relevant to industrial infrastructure (Ahmad et al., 2015, Guo et al., 2017), including comprehensive approaches aimed at modelling and investigating the generation of CO_2 solids during decompression of a pipeline system across the triple point (Zheng et al., 2017). Li et al. (Li et al., 2018) undertook an ejection process of boiling and swelling of the pressurized liquid CO_2 (3-5 MPa) following vessel rupture and found that within 20 ms, the pressure peaks surpassed the initial values and constituted the beginning of a CO_2 Boiling Liquid Expanding Vapour Explosion (BLEVE). During a BLEVE, the rupture of a vessel leads to an abrupt depressurisation of liquid inventory stored under pressure. As a result, the thermodynamic equilibrium present under storage conditions becomes inherently unstable, and temperature increases above saturation temperature. The fluid reaches a superheated liquid state, thus evaporating at a rapid rate and generating a large volume increase. This causes a significant displacement of ambient air, and a blast wave that propagates to the surroundings (Bjerketvedt et al., 2011, Van der Voort, 2013, Tosse et al., 2015). A BLEVE accident took place in Worms, Germany in 1988 when the failure of a CO_2 liquid tank culminated in three fatalities, three months production loss and considerable infrastructural damage (Van der Voort, 2013). A more moderate BLEVE accident also took place in Norway in 2008, when a fire extinguisher containing 5 kg of liquid CO_2 was sent to be shredded as part of its disposal process in a waste bin. The operation punctured the cylinder, causing it to violently burst into several fragments that travelled over 30 m away (Van der Voort, 2013). Conversely, a relatively limited number of studies have scrutinised accidental leakage behaviour of CO_2 under conditions typical of ship transport (Han et al., 2013, Han et al., 2014, Al Baroudi et al., 2021b, Shafiq et al., 2018). In these regards, it is noteworthy that generation of solids and propensity for blockages during leakage behaviour of CO_2 under refrigerated liquid state (0.7 – 2.6 MPa, 223 – 263 K) is largely affected by the margin of initial conditions from the triple point (0.51 MPa, 217 K) (Al Baroudi et al., 2021b). When it comes to the transportation of compressed, refrigerated CO_2 by ship, significant experience can be gained from the liquefied natural gas (LNG) and liquefied petroleum gas (LPG) industries (WorleyParsons et al., 2009).

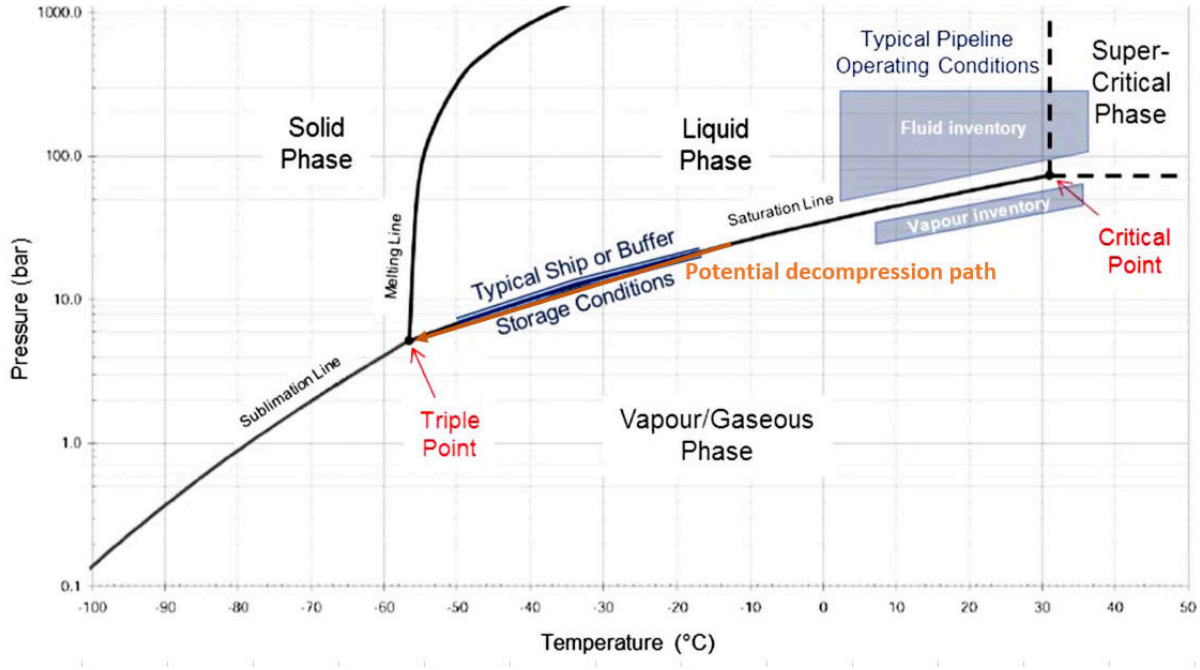

Fig. 1 Carbon dioxide phase diagram with typical transport conditions and potential decompression path during release. Adapted from Holt et al. (2012)

Cargo carriers include semi-pressurised, fully pressurised and fully refrigerated ships depending on the intended pressure and temperature conditioning (SIGTTO, 2016). As part of the CO_2 shipping chain, marine loading operations are performed at the onshore or offshore terminals by means of cryogenic loading arms, representing the most established solution (Al Baroudi et al., 2021a; Vermeulen, 2011; Chiyoda Corporation, 2012). In order to reduce the risk associated with the transfer of refrigerated, liquefied inventory, several studies (Vermeulen, 2011; WorleyParsons et al., 2009; Koers, 2011; Zahid et al., 2015; Pitbaldo et al., 2004) and standards (SIGTTO, 2017) emphasised that the installation of Emergency Shutdown Valves (ESDV) to isolate the damaged areas and Emergency Release Systems (ERS) can protect the loading arm (Fig. 2). ERS are extensively used in marine loading applications in the oil and gas industry (Pitbaldo et al., 2004; California State Lands Commission, 2006; SIGTTO, 2017), and are designed to disconnect the loading arm from the ship during operations in the event emergencies such as natural calamities, fire disaster and strong wind or current that causes sudden movement of the ship away from the berthing line.

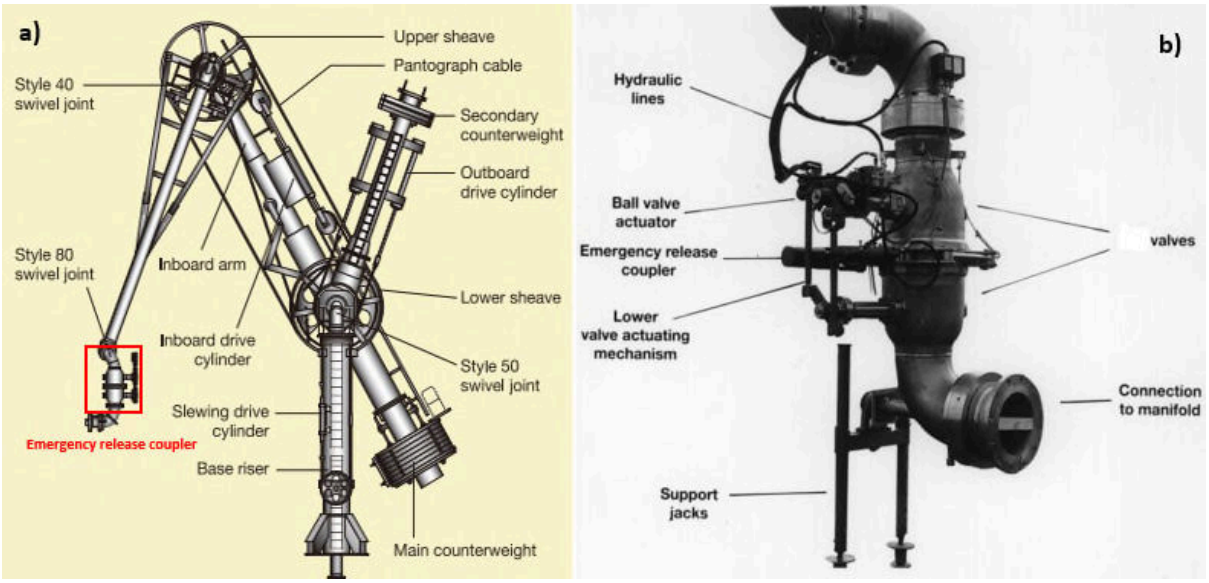

Fig. 2 a) Schematic representation of marine loading arm with integrated emergency release coupler (Tokyo Boeki Engineering, no date); b) specific design features of an emergency release coupler (SIGTTO, 2016)

The system is comprised of two valves, one located at the loading arm's side, and the other at the ship's side (Fig. 2). As illustrated in Fig. 3, during an emergency the two valves will close simultaneously to avoid spillage of inventory. An emergency release coupler, representing the interface between the two valves, is therefore operated by means of a pressurised fluid reservoir, and disconnects the loading arm immediately after closure of the valves (Fig. 2). As part of the ERS design, an interlock system is integrated to ensure that the decoupling of the arm only occurs upon closure of both valves, thus limiting the spillage to a few litres as per emergency coupler's design. Emergency Release Systems designed by Tokyo Boeki Engineering take up to 5 s to respond to the anomaly value and a further 2 s to open and release the coupler, for a total cumulative action time of 7s. ERS's can be operated both manually, or by means of control systems that detect anomalies in the loading operations and cut off the supply of inventory. In both scenarios, it is critical to understand the impact of liquid CO_2 discharge in order to develop appropriate design codes and safety protocols. In these regards, the California State Lands Commission (California State Lands Commission, 2006) reported that 10 out of 52 major LNG accidents taking place between 1944 and 2006 occurred during loading and offloading operations, with significant property damage and spillage taking place in all the occurrences. The Society of International Gas Tankers and Terminal Operators (SIGTTO) (SIGTTO,

2017) highlighted that in the period comprised between 1995 and 2017, 32 spurious activations of the ERS were reported, mostly attributed to equipment failure or operational malfunctions.

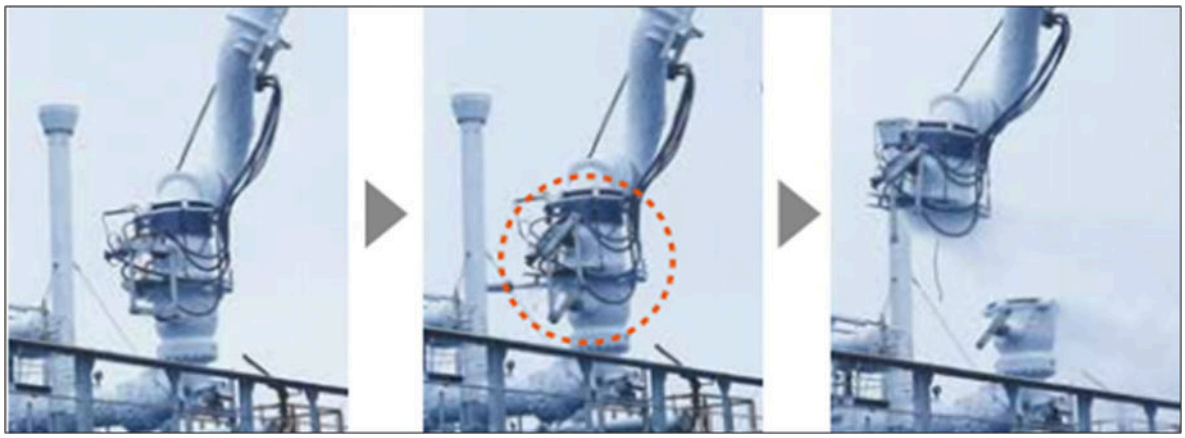

Fig. 3: Sequence of the operation of ERS; 1) separation begins; 2) the two valves shut completely; 3) Emergency Release Coupler opens completing the separation (Tokyo Boeki Engineering, n.d.).

For a safe and efficient design and operation of the systems, a thorough understanding of the phenomena is necessary. Although emergency release systems are well established in LNG and LPG industries (SIGTTO, 2016), their application to liquefied CO_2 applications is not well understood. Carbon dioxide is expected to behave differently than any of the former applications, as it can only be liquefied by pressurisation above its triple point pressure of 0.51 MPa. Continuous handling during marine loading operations requires a thorough understanding of the potential for sublimation and generation of solid CO_2 (dry ice) during an emergency shutdown, which can result in equipment becoming irresponsive. These features are unique to carbon dioxide, making the discharge behaviour unpredictable (Energy Institute, 2013; Noh et al., 2018). Table 1 summarises and compares the difference in typical operating conditions of different liquefied gas carriers along with the triple point of the fluids.

Table 1 Typical transport conditions and triple point condiitons of different liquefied gases

Liquefied gas	Typical transport pressures (MPa)	Typical transport temperatures (K)	Triple point conditions	Source
LNG	0.1	112	0.1 MPa, 91 K*	Worley Parsons (2013)
LPG	0.1 - 2	227 - 298	0.1 MPa, 85 K** 0.1 MPa, 135 K***	Luketa and Hightower (2018)
LCO_2	0.6 – 1.9	218 - 259	0.51 MPa, 217 K	Element Energy (2018)

*value relative to methane – primary component of LNG
**value for propane – one of the primary components of LPG
***value for butane - one of the primary components of LPG

Therefore, this work presents a real-scale investigation of the discharge of liquefied, refrigerated carbon dioxide from an emergency release coupler under conditions relevant to large-scale CO_2 shipping. The aim is to scrutinise the applicability of the existing ERS technology used in LNG and LPG applications to liquid CO_2 carriers and understand the implications associated with the selection of either low or medium pressure conditions. In these regards, the study undertakes qualitative observations and diagnostics of the phenomena with the aim of understanding their nature and the impact on the design, material considerations and process safety, including dispersion of the jet flow and solids formation. Findings are aimed at advising on the design and operation of emergency release systems for liquid CO_2 carriers.

2 Methodology

2.1 Experimental set-up

The cryogenic test facility is represented in Fig. 4, commissioned to simulate the operation of an emergency release system during a shutdown. The facility features a stainless-steel cylindrical test vessel, with internal diameter of 249 mm and height of 134 mm, making its volume ~6 litres as shown in Fig. 6. These dimensions are equivalent to the butterfly-valve emergency coupler of an 8-inch size marine loading

arm as designed by Tokyo Boeki Engineering, thus making this a real-scale investigation of CO_2 release during an emergency shutdown. The test vessel was insulated using a polyethylene AEROFLEX and glass wool insulation. The feed and set pressure of the CO_2 were controlled at the source by means of a throttling valve fitted on the carbon dioxide supply tank (2 MPa and 253 K) while carbon dioxide flow across the facility was controlled though the installation of ball valves.

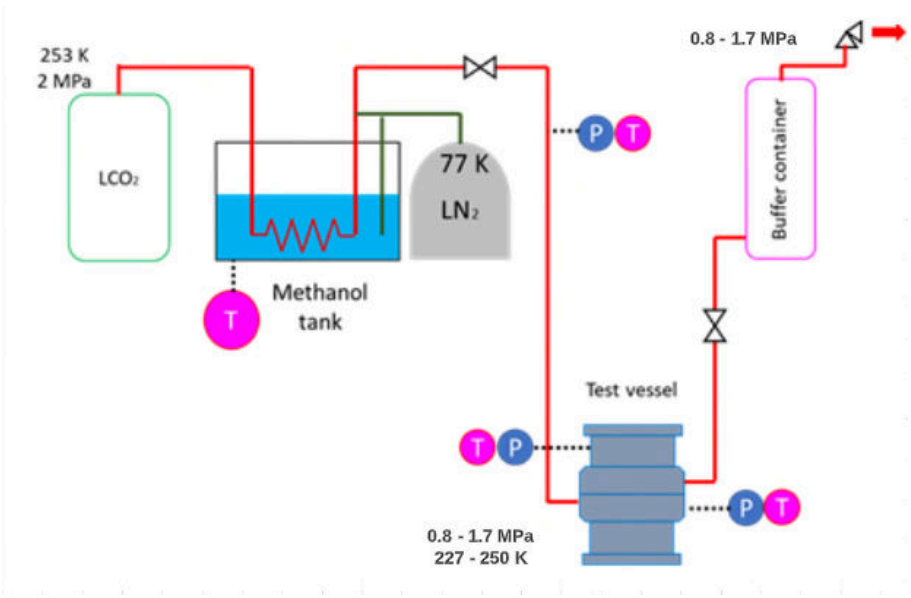

Fig. 4: Schematic representation of the test facility

Moreover, a buffer container was placed after the vessel's outlet to allow for the venting of any excess pressure from the vessel during the test preparation (Fig. 4). A methanol-liquid nitrogen refrigeration system was used to condition the liquid CO_2 to the required temperature prior to injecting it into the cylindrical vessel. Fig. 5 presents a graphical representation of the experimental facility.

Fig. 5: Pictures of the experimental apparatus - left-to-right and top-to-bottom: test vessel; methanol-nitrogen refrigeration; buffer container; inlet, outlet pipework and pressurised oil system

A hydraulic system was implemented to enable the vertical separation of the test vessel required for the experimental tests (Fig. 6), representing hydraulic lines present in real ERS systems for coupler disconnection (Fig. 2). The system was operated at constant flowrate through a pressurised oil reservoir that drives the cylinder strokes, allowing for the opening and closing of the pressure cylinder. This results in a total separation distance of 400 mm of the decoupler test vessel, which takes place over approximately 7 s from its triggering at a uniform rate. It is assumed that the rate of vessel's opening will only be controlled by the hydraulic system and that the effect of pressure exerted by the fluid can be considered negligible. Extensive temperature measurements were acquired through Hayashi Denko k-type thermocouples with 1 mm diameter (106 – 240 K measuring range, ± 0.05 K) with a reported response time of 0.02 s in water media. Pressure acquisition was performed by means of Keyence GM-P025T pressure sensors (0.1 – 2.5 MPa ± 0.01 MPa with response time of 0.01

s) fitted across the facility (Fig. 4) to allow a real-time monitoring and data acquisition (5 Hz rate, selected based on the maximum capacity of the data acquisition system).

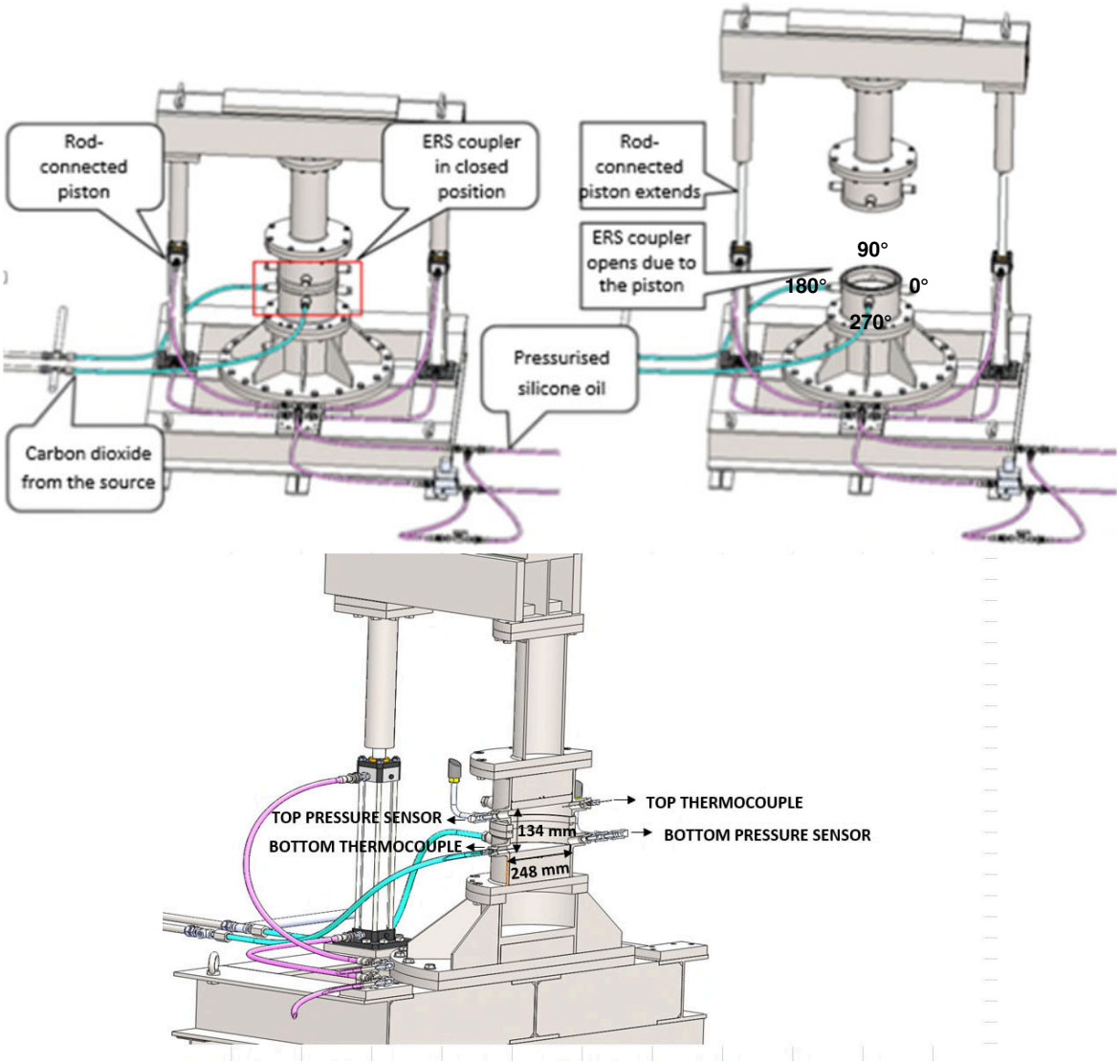

Fig. 6 Illustration of the test vessel experimental system operating principles (top); internal structure, dimension, and measurement location of the test vessel (bottom)

A high-frame camera (240 fps) was placed at approximately 15 m away from the test facility at an elevated height to capture the dispersion of the jet. A GoPro camera (120 fps) was fitted on the top bracket of the test facility to allow for a top-view observation of the phenomena during the test. Moreover, a high-speed camera with a capture rate of 960 fps was placed 2.5 m in front of the test vessel to observe the discharge in slow-motion. The captured frames are then used to determine the initial speed of the jetted flow in the first instances of the discharge. An infrared thermography AVIO R500EX with a temperature range of 233 to 773 K and video capture rate of 30 fps was obtained

to record the thermal profile of the release; the emissivity value was selected to be 0.95 for this application. The IR thermography was placed next to the high-speed camera at 2.5m from the test vessel in test 1.1 and test 2.1 to promote a thorough observation of the discharge phenomena.

2.2 Experimental schedule

Four real-scale tests are considered to investigate the operation of the emergency release coupler and the discharge behaviour of industrial-grade CO_2 (minimum 99.5% purity) with a range of experimental diagnostics as summarised in Table 2. The experimental campaign focuses both on low pressure (0.6–1 MPa) and medium pressure conditions (1.5 – 1.9 MPa) considered for future large-scale CO_2 shipping projects (Al Baroudi et al., 2021a, Element Energy, 2018, Ministry of Petroleum and Energy Norway, 2016). Tests 1.1 and 1.2 are performed at low pressure shipping conditions of 0.87 MPa and 0.96 MPa respectively, in proximity of the triple point and solid region (see Fig. 17); the initial liquid CO_2 temperature is selected to be within 2 K below the corresponding saturation temperature. Conversely, tests 2.1 and 2.2 are considered at medium pressure CO_2 shipping conditions (1.62 – 1.65 MPa) exhibiting a wider margin from the triple point (Fig. 18); the initial CO_2 temperature was hereby chosen to be 6 – 7 K below saturation temperature in order to investigate the impact of a more considerable margin from the saturation line and vapour phase. Table 3 provides a summary of conditions scrutinised in this experimental campaign.

Table 2: Summary of experimental observations and data acquisition; TC = thermocouple PT = pressure transducer. Colour coding: green indicates present diagnostic while red indicates absence of diagnostics

Test	Top and Bottom TC and PT in test vessel	High-speed camera	Far-view camera	Top-view – GoPro camera	Thermal IR camera
Test 1.1					
Test 1.2					
Test 2.1					
Test 2.2					

Table 3: Summary of the experimental schedule

Test	Pressure (MPa)	Temperature (K)	Initial methanol temperature (K)	Ambient temperature (K)
Test 1.1	0.87	227	221	289
Test 1.2	0.96	231	222	288
Test 2.1	1.65	239	224	280
Test 2.2	1.62	240	226	281

3 Results and Discussion

3.1 Observation of the discharge phenomena

During the vertical separation of the vessel, the high-speed acquisition (Fig. 7) shows that the release at 0.96 MPa occurs in a progressive manner and in several stages. At 4 ms from the start of the separation, a low-momentum leak lasting 8 ms discharges from the 0° section (as defined in Fig. 6) of the opening; the vessel continues to separate vertically, and at 50 ms from the start a uniform leak discharge throughout the whole cylinder's circumference, effectively initiating the full discharge.

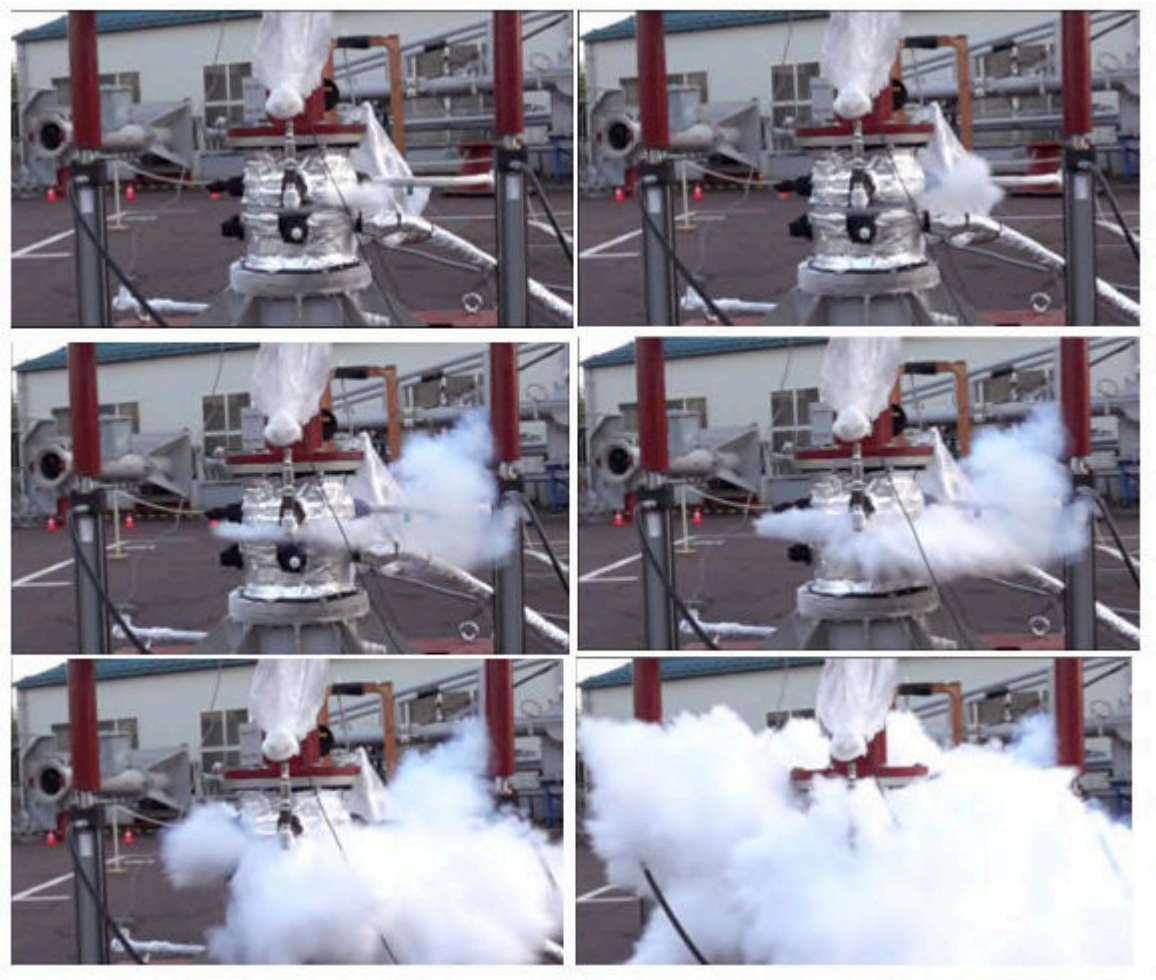

Fig. 7: Frame sequence of high-speed release of Test 1.2; left-to-right and top-to-bottom 4 ms, 8 ms, 50 ms, 53 ms, 55 ms and 73 ms

Conversely, Fig. 8 shows that the discharge behaviour at the higher pressure of 1.65 MPa is more sudden, with immediate discharge within 4 ms from the 180° section of the opening (defined in Fig. 6) and progressive spreading across the full circumference within 8 ms. As shown in Fig. 9, accumulation of solid CO_2 (dry ice) was found on the surface of the vessel immediately upon completion of both tests. Qualitative observation shows that a larger amount of dry ice may have formed under low pressure conditions (test 1.2, 0.96 MPa) as opposed to medium pressure (test 2.1, 1.65 MPa) which only shows a modest layer with no significant localised accumulation. During emergency shutdowns, the ability to operate without the effects of residues is essential, because formation of solid CO_2 can potentially cause valves to become irresponsive (Energy Institute, 2010), and disrupt the disconnection of the emergency coupler (represented in Fig. 3). As shown in Fig. 9, at the end of test 1.2 (0.96 MPa), the O-ring was found to be shifted sideways at the bottom of the coupler, while after

the completion of test 2.1 (1.65 MPa) the O-ring was fastened around the outside circumference of the lower half of the vessel.

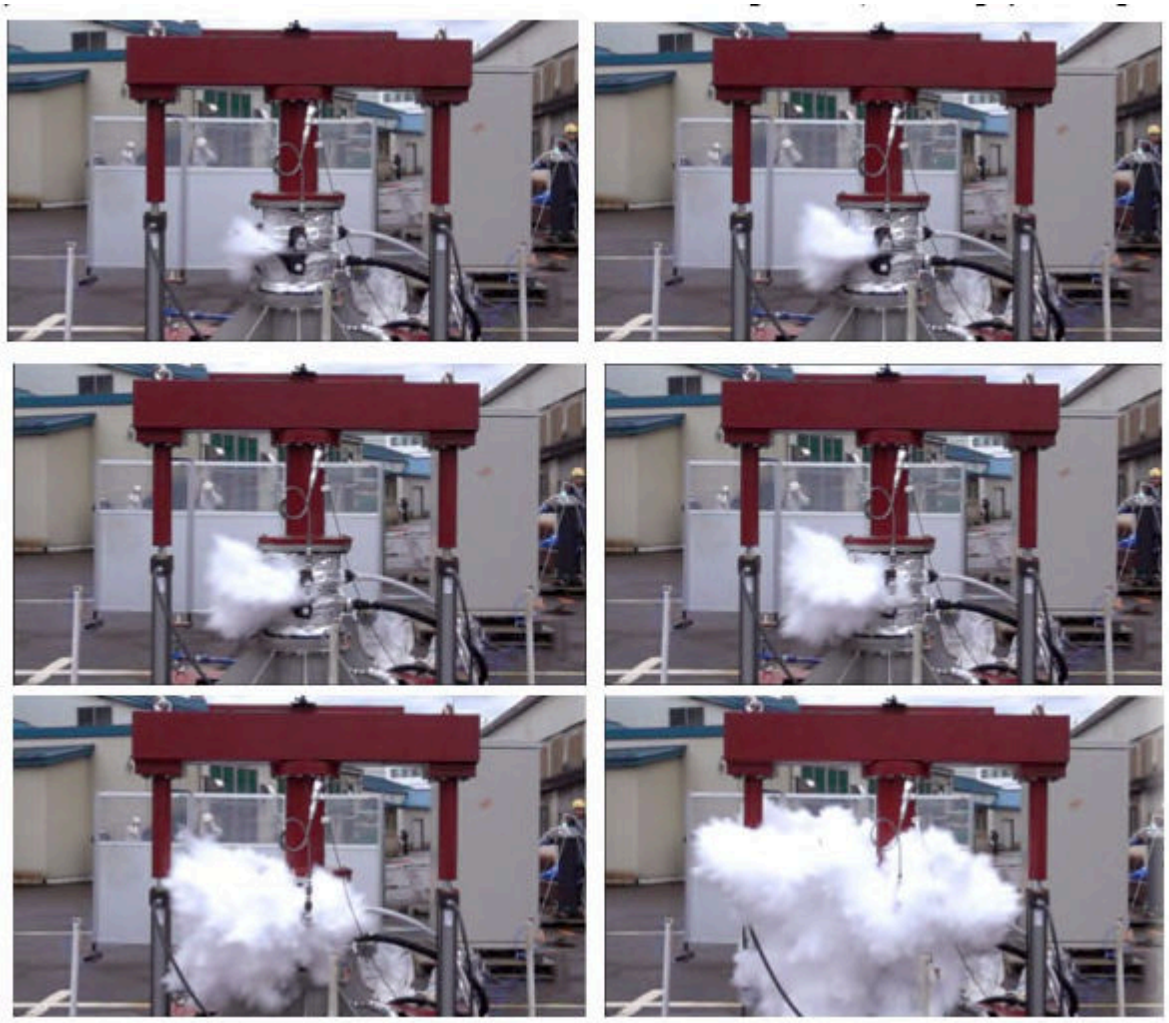

Fig. 8: Frame sequence of high-speed release of Test 2.1; left-to-right and top-to-bottom 4 ms, 6 ms, 7 ms, 8 ms, 11 ms and 16 ms

Fig. 9: Bottom surface of the test vessel after the experiment; Test 2.1 (left), Test 1.2 (right)

Given the lower pressure of CO_2, the residual gasket load is higher in test 1.2 than test 2.1, resulting in a more robust seal. In test 2.1 (1.65 MPa pressure) the friction and compression force between the flanges are rapidly overcame as the vessel begins vertical separation, and the O-ring spreads at a stretch under the effect of the internal pressure, causing CO_2 to violently leak from the circumference. On the other hand, in test 1.2 performed at 0.96 MPa initial pressure, the net compression force between flanges is relatively higher due to lower fluid pressure. Therefore, as the vessel begins vertical separation, the equilibrium between the two forces involved in the flange assembly results in a slower spread of the seal that can be explained by the final position of the O-ring. This reconstruction is supported by the top-view camera observation shown in Fig. 10, which shows that in test 1.1 an initial puff delays the full discharge phenomena, whilst the outflow behaviour in test 2.1 appears to be immediate.

Fig. 10: Top view of the release of Test 1.1 (left) and Test 2.1 (right) after 0.01 s of the vessel separation

3.2 Discharge behaviour of liquid CO_2 from the test vessel

The pressure profile of liquid CO_2 in the performed tests shows that the test vessel reaches atmospheric pressure within 0.4 – 0.6 s of the start of the release under the low-pressure condition (tests 1.1 and 1.2 at 0.87 – 0.96 MPa, shown in Fig. 11) and within 0.4 s in the medium pressure conditions (tests 2.1 and 2.2 at 1.62 – 1.65 MPa, shown in Fig. 12). Under low pressure conditions, the depressurisation from the vessel occurs more gradually, achieving its peak rate of 2.8-3.5 MPa s^{-1} (recorded at the top of the vessel) after 0.4 s from the start of the release. Moreover, a significant difference in maximum depressurisation rate is observed among the top and bottom parts of the vessel as shown in Fig. 11. Conversely, the behaviour under medium pressure conditions (test 2.1 and 2.2, 1.62 – 1.65 MPa) is associated with an abrupt depressurisation whereby the peak rate of 5-6 MPa s^{-1} (recorded at the top of the vessel) is achieved after 0.2 s, as shown in Fig. Under these conditions, a more uniform depressurisation rate between the top and the bottom of the coupler is observed (Fig. 12). It should be noted that the depressurisation rates are correlated with the sampling frequency of the recording, set to 5 Hz in this study. This aimed at outlining a comparison between the pressure profile between low (test 1.1 and 1.2) and medium (2.1 and 2.2) pressure conditions, and it is emphasized that specific values will differ depending on the selected acquisition rate.

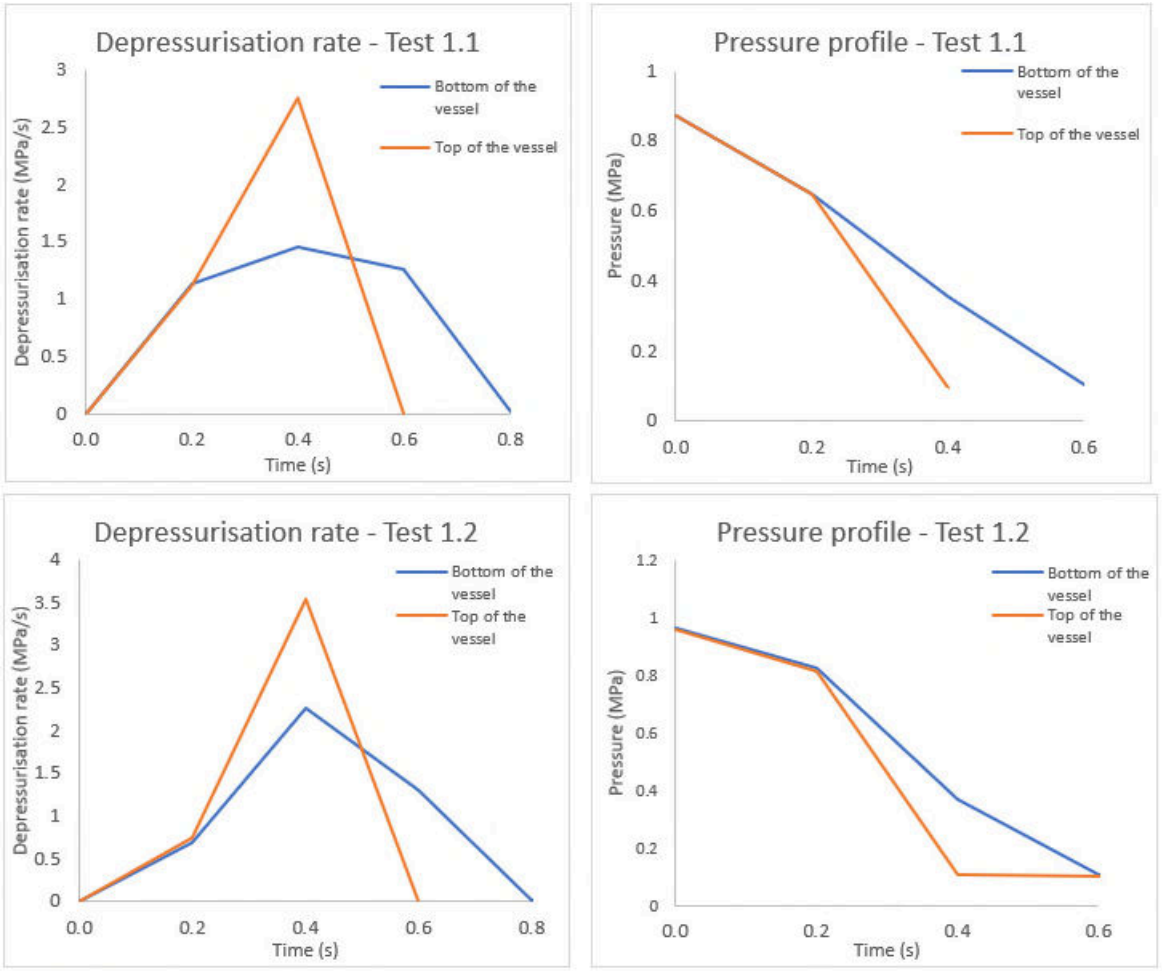

Fig. 11: Pressure profile and depressurisation rate in the tests 1.1 and 1.2

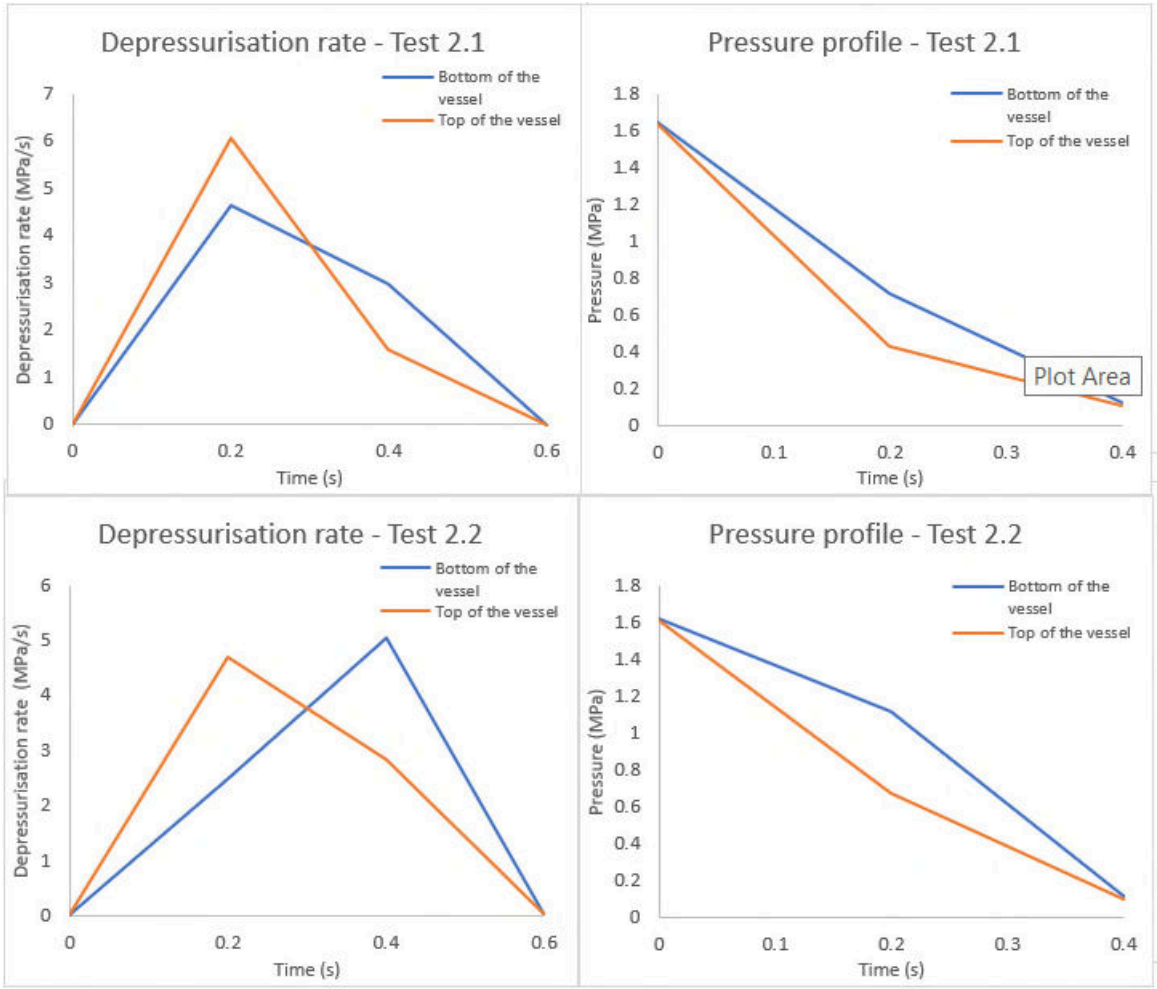

Fig. 12: Pressure profile and depressurisation rate in tests 2.1 and 2.2

During initial storage conditions, carbon dioxide liquid and vapour phase inside the test vessels are in thermodynamic equilibrium. As the test vessel is vertically separated (Fig. 6), the liquid rapidly starts to boil from the surface in an endothermic process until reaching atmospheric pressures. The phenomenon induces a further temperature decrease in the liquid, which leads to partial condensation and freezing of the carbon dioxide. This was observed in the form of dry ice accumulation on the surface of the test vessel as shown in Fig. 9. The abrupt phase transition from liquid to vapour causes a remarkable volume increase that displaces ambient air, generating a blast wave in all performed tests that could be heard from afar. During the vessel separation, the depressurisation at the top of the vessel shows higher rates than the bottom, as reflected in Fig. 11 and Fig. 12. As established in the earlier paragraph, the forces acting between the vessel's flanges and the fluid's vapour pressure results in a relatively faster separation of the test vessel in the scrutinised medium pressure condition (test 2.1) compared to the low pressure one (test 1.2). The behaviour is

hereby attributed to the boiling of the saturated liquid during the liquid-vapour phase transition, thus sustaining the pressure. In tests 2.1, this behaviour is less obvious and the discrepancy between the top and the bottom pressure profile in the coupler is less remarkable, owing to the more uniform discharge during test vessel separation. In order to observe the early stage of the jet release from the test vessel, velocity values were measured based on the video recording (960 fps), referring to the visible CO_2 cloud escaping in the radial direction with respect to time during the vertical separation of the coupler, as shown in Fig. 7 (test 1.2) and Fig. 8 (test 2.1). Values of the radial displacement of the jet and its velocity were determined through the calibrated measurement of the high-speed camera frames, taken starting from 1 ms of the start of the release at intervals of 1 ms. Fig. 13 shows the measured velocity profile of the inventory discharges in test 1.2 and test 2.1. As previously reported, the irregular slip initiation of the gasket seal encountered at a lower pressure leads to a lower-momentum puff prior to the full blast. The initial leak discharges from the 180° side of the opening, exhibiting an ejection speed of approximately 34 m s^{-1}. The remainder of the inventory begins to discharge from the 0° side of the opening at an initial speed of 115 m s^{-1}, which drops to 64 m s^{-1} after 2 ms (Fig. 13). Conversely, the discharge at test 2.1 (medium pressure condition of 1.65 MPa) exhibits a more uniform profile, with no initial leaks taking place. There, the speed progressively reduces from an initial value of 149 m s^{-1} at 1 ms to a mere 60 m s^{-1} after 2 ms.

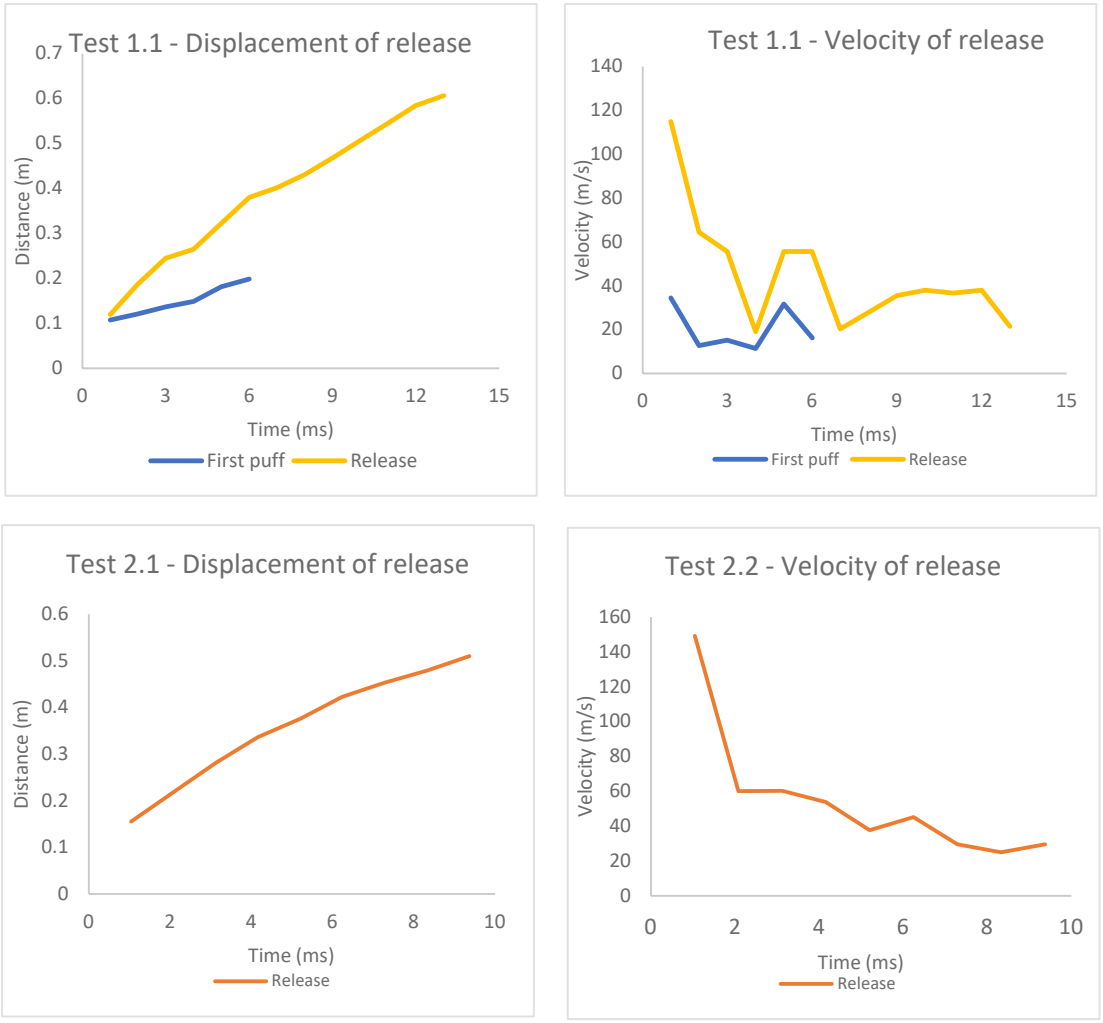

Fig. 13: Measurement of the jet speed in tests 1.2 and 2.1

3.3 Temperature profile

Fig. 14 shows the temperature profile inside the coupler's top and bottom during all the tests. As it can be observed, temperatures as low as ~ 185-190 K are reached in the test vessel within approximately 3 s of the start of the discharge in all tests. This will have clear implications on material selection associated with the design and construction of emergency release couplers, whereby candidate materials will need to perform satisfactorily at such temperatures without the risk of embrittlement and failure. Brevik Engineering AS (Brevik Engineering AS, 2020) provided a list of steel grades – including P355NL1 and ASTM A203 F and VL 9Ni – relevant to the construction of refrigerated CO_2 pressure vessels with minimum design vapour pressure of 0.8 MPa; however, it should be noted that these materials are only suitable for minimum design temperatures of 218 K. Similarly, Seo et al. (Seo et al., 2016) identified ASTM A537 heat treated carbon for the construction of CO_2 storage

pressure vessels, though this is only deemed appropriate for temperatures down to 223 K. As shown in Fig. 14, the campaign highlighted that higher rates of temperature drops (32 K/s and 40 K/s maximum value, respectively) occur under medium pressure conditions (tests 2.1 and 2.2, 1.62 – 1.65 MPa) compared to low pressure tests (tests 1.1 and 1.2, achieving 20 K/s and 22 K/s maximum value respectively). This behaviour can be attributed to the Joule-Thomson (JT) effect, a thermodynamic behaviour that governs real gases, describing their temperature change correlated with an isenthalpic expansion where no heat or work is exchanged with the surroundings. The JT coefficient (μ_{JT}) can be expressed as:

$$\boldsymbol{\mu_{JT}} = \left(\frac{\partial \mathbf{T}}{\partial \mathbf{P}}\right)_{\boldsymbol{H}} \quad 1$$

Given the larger pressure difference between medium pressure conditions (test 2.1 and 2.2) and atmospheric pressure, the corresponding total temperature drop recorded in the test vessel is also higher than that under low pressure conditions (test 1.1 and 1.2) as shown Fig. 14. Fig. 15 and Fig. 16 show the thermal imaging profile of the jet surrounding the test vessel in tests 1.1 and 1.2 respectively. Due to the higher residual gasket force and initial low-momentum leak encountered at lower pressures – explained in the previous paragraphs - test 1.1 shows an overall slower discharge process, with an initial puff at 0.07 s. The jet surrounding the test vessel shows the peak of its discharge between 0.2 s – 0.27 s, where a cloud exhibiting temperatures of approximately 243 - 248 K dissipates and progressively warms up (Fig. 15). At 0.8 s and 1.33 s, localised low temperature area can be observed in proximity of the bottom of the test vessel, representing formation of solid CO_2 (dry ice). The thermal profile of the cloud surrounding the test vessel in test 2.1 conversely shows a faster release and dispersion process, starting from 0.03 s. The cloud surrounding the test vessel reaches its lowest temperature – recorded below 233 K (minimum temperature range of the thermal camera) - between 0.1 s - 0.17 s from the start of the release.

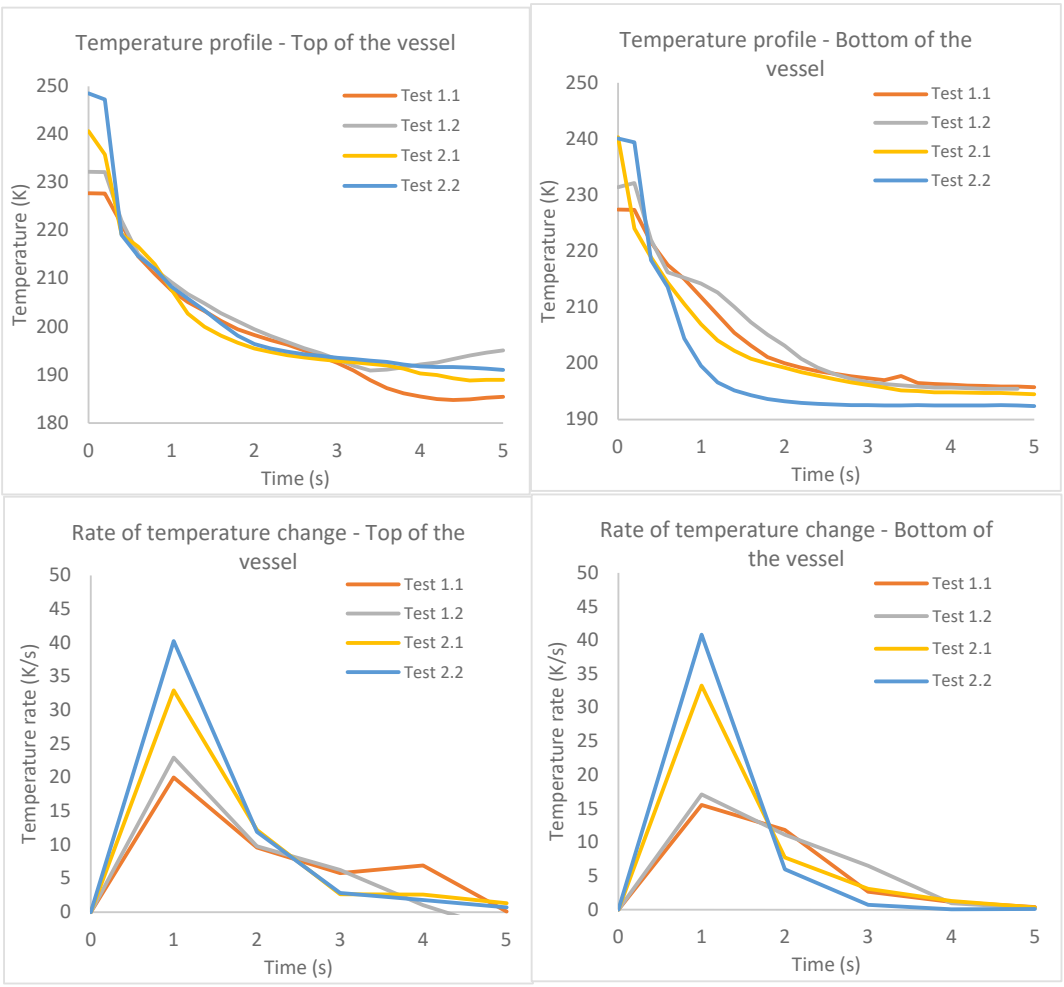

Fig. 14: Temperature profile inside of the coupler in the test

After that point, the area in the vicinity of the test vessel shows a progressive increase in temperature, attributed to the dissipation of the cloud and rapid air entrainment. Similarly, to what encountered in test 1.1, a localised low temperature area is observed near the bottom of the coupler at 0.3 – 0.73 s, indicating solid CO_2 formation as presented earlier in this work (Fig. 9).

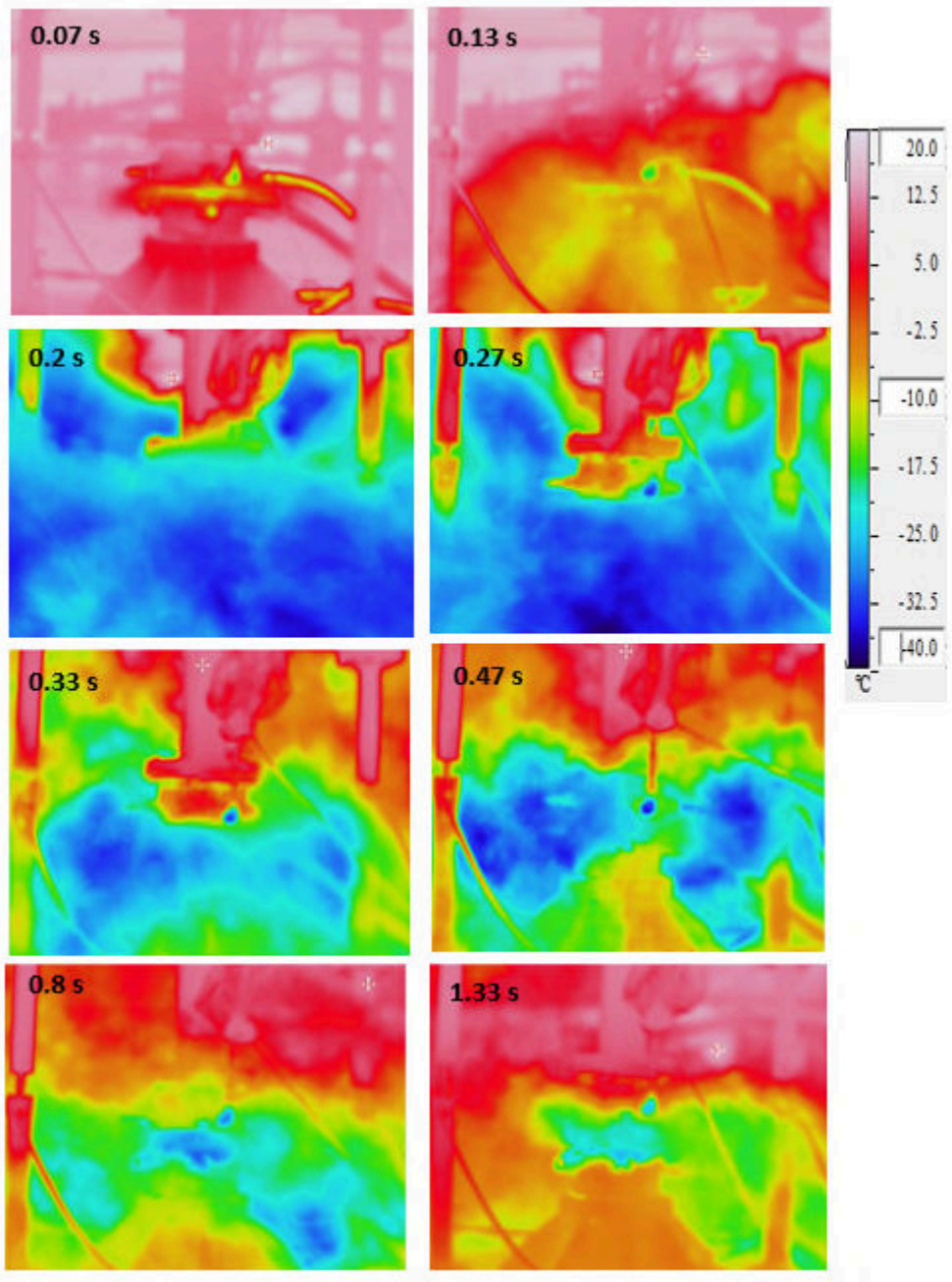

Fig. 15: Thermal imaging profile of the discharge in Test 1.1

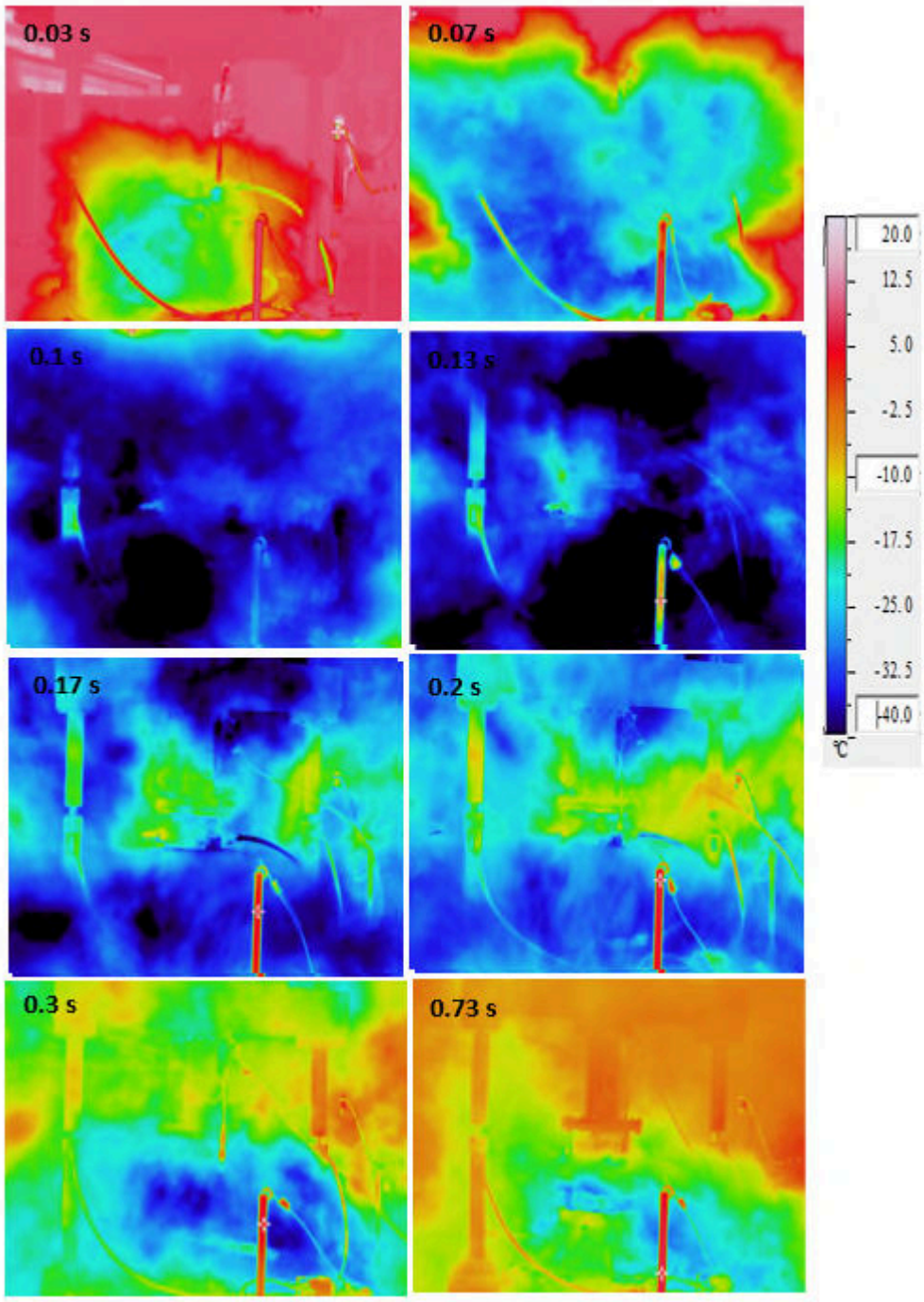

Fig. 16: Thermal imaging profile of the discharge in Test 2.1

3.4 Dispersion and dry-ice formation

The path of release under low pressure (test 1.1, 0.87 MPa) and medium pressure conditions (test 2.1, 1.65 MPa) are shown in Fig. 17 and Fig. 18 respectively. This reconstruction is obtained by plotting on the CO_2 phase diagram the recorded pressure and temperature values for time-specific data sets throughout the discharge. The plots show that under both low and medium pressure, the carbon dioxide transitions from

liquid to vapour state within 0.2 s of the start of the discharge and enters the solid equilibria within 2.8 – 3 s, when no CO_2 inventory is left in the vessel and dry ice formed during the expansion process accumulates on the surface of the test vessel (as described in section 3.2). Solid CO_2 phase therefore begins to exchange heat with the surroundings, progressively sublimating away from the test vessel. Thermodynamic theory (Ekeberg, 2015) states that when the CO_2 jet undergoes isenthalpic expansion, eventually reaching the triple point pressure (0.51 MPa), a fraction of the CO_2 will

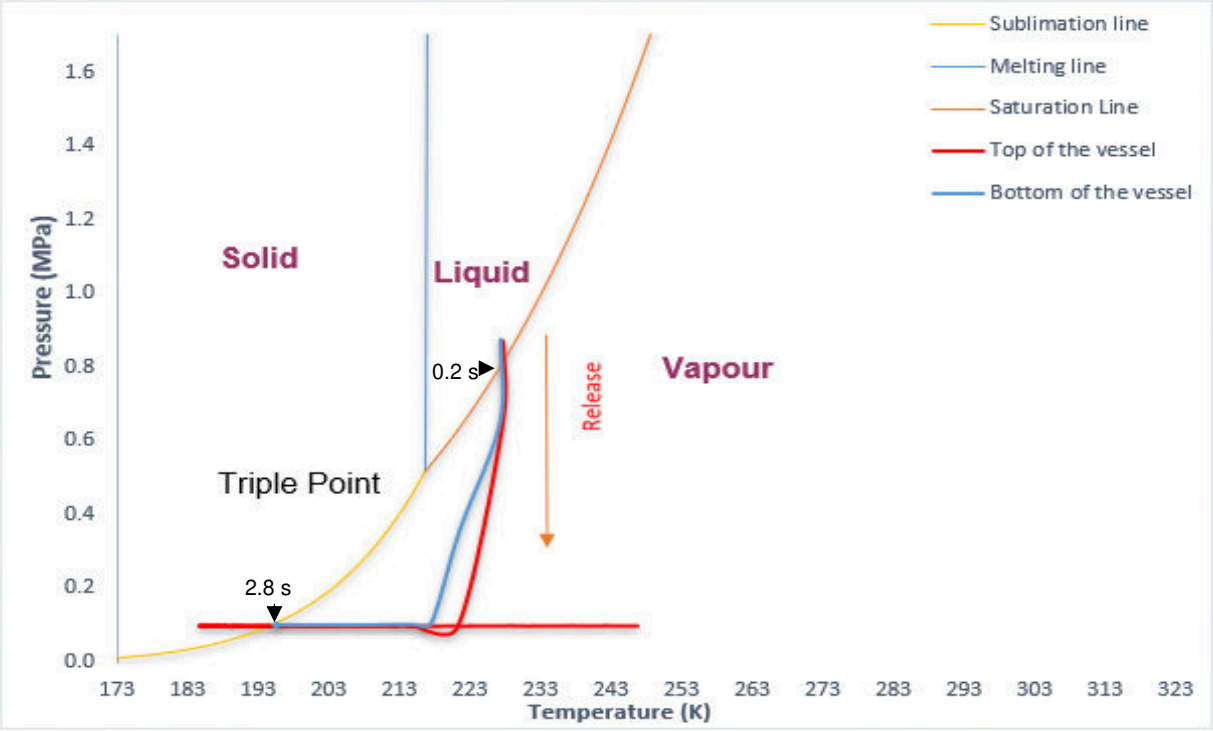

Fig. 17: Phase diagram of the release in Test 1.1

transition from gaseous to a solid state, and solids will scatter around the test vessel in powdery form (Fig. 19). Assuming an isenthalpic expansion, the generated solid fraction is mainly dependant on upstream specific enthalpy values of the fluid under storage conditions (Energy Institute, 2010).

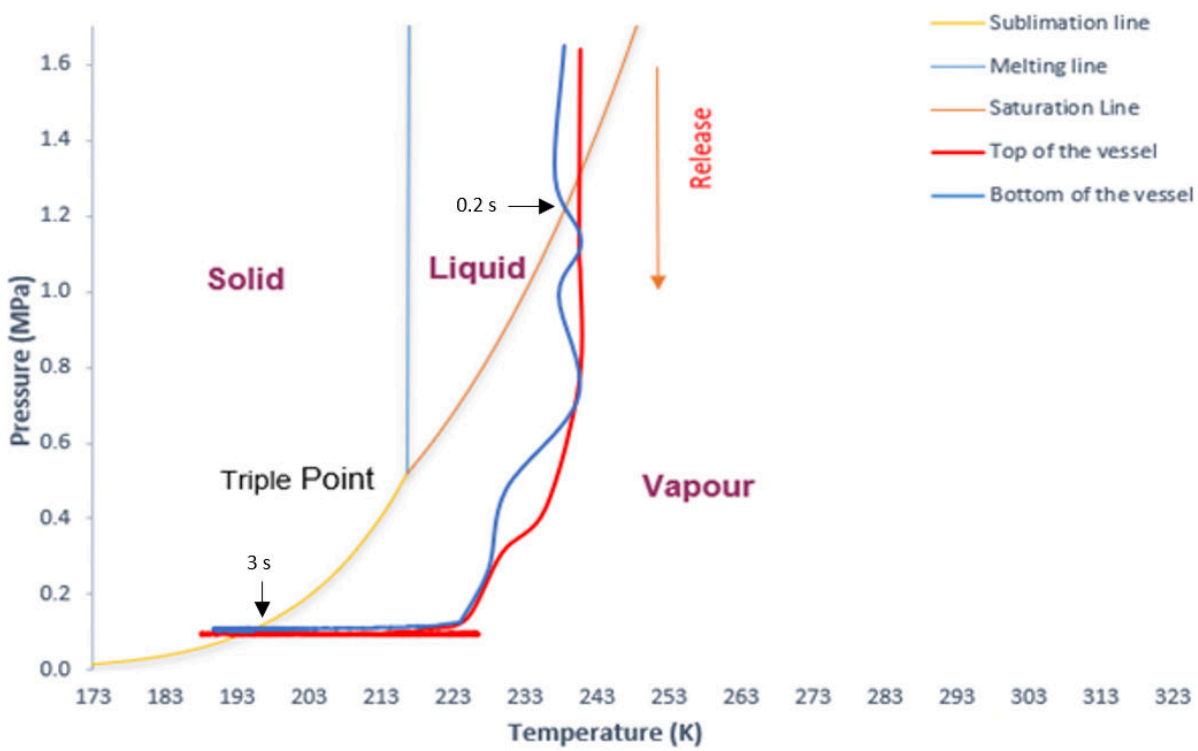

Fig. 18: Phase diagram of the release in Test 2.1

The release behaviour in the region immediately adjacent to the exit plane is explained by the simplified method employed by Fauske and Epstein, described in detail in the Energy Institute report (Energy Institute, 2010). As illustrated in Fig. 20, beyond the exit plane, the jet enters a depressurisation zone during its isenthalpic expansion, where no entrainment of air occurs due to pressure being higher than atmospheric. Therefore, the stream enters a two-phase gaseous and solid entrainment zone, where pressure equilibrates with atmospheric conditions ($\boldsymbol{P_2 = P_{atm}}$.)

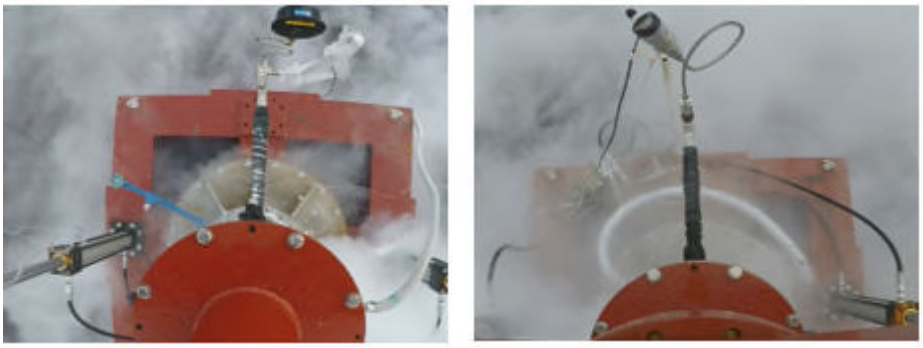

Fig. 19: Top view of the post-test release; Test 1.2 (left) and Test 2.1 (right)

Principles of energy, momentum flux and mass conservation are applied to determine the properties of the jet at the end of the depressurisation zone (Energy Institute,

2010). The process is considered isenthalpic (no exchange of heat with the surroundings), and a further simplification (Energy Institute, 2010) elaborates that the velocity terms can be neglected, thus giving $\boldsymbol{h_2 = h_1}$ (Fig. 20). The correlation between enthalpies and mass fraction split between solid and gaseous phase is summarised as:

$$\boldsymbol{h_1 = h_2 = h_{s,1} + Y_{g,1} h_{sg,1} = h_{s,2} + Y_{g,2} h_{sg,2}} \quad (2)$$

Where Y_g represents the split vapour mass, $h_{sg,1}$ and $h_{sg,2}$ are the difference between solid and gaseous enthalpy at atmospheric pressure. The equation can be rearranged to give the split solid fraction (Y_s) at the end of the depressurisation zone as the subject:

$$\boldsymbol{Y_s = 1 - \left(\frac{h_2 - h_s}{h_{sg}} \right)} \quad (3)$$

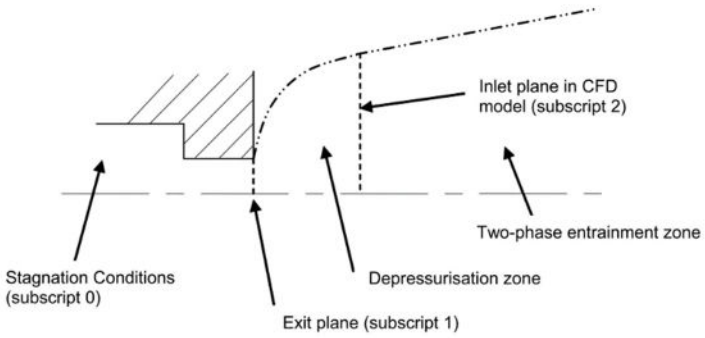

Fig. 20: Simplified schematic of the release at the exit (Energy Institute, 2010).

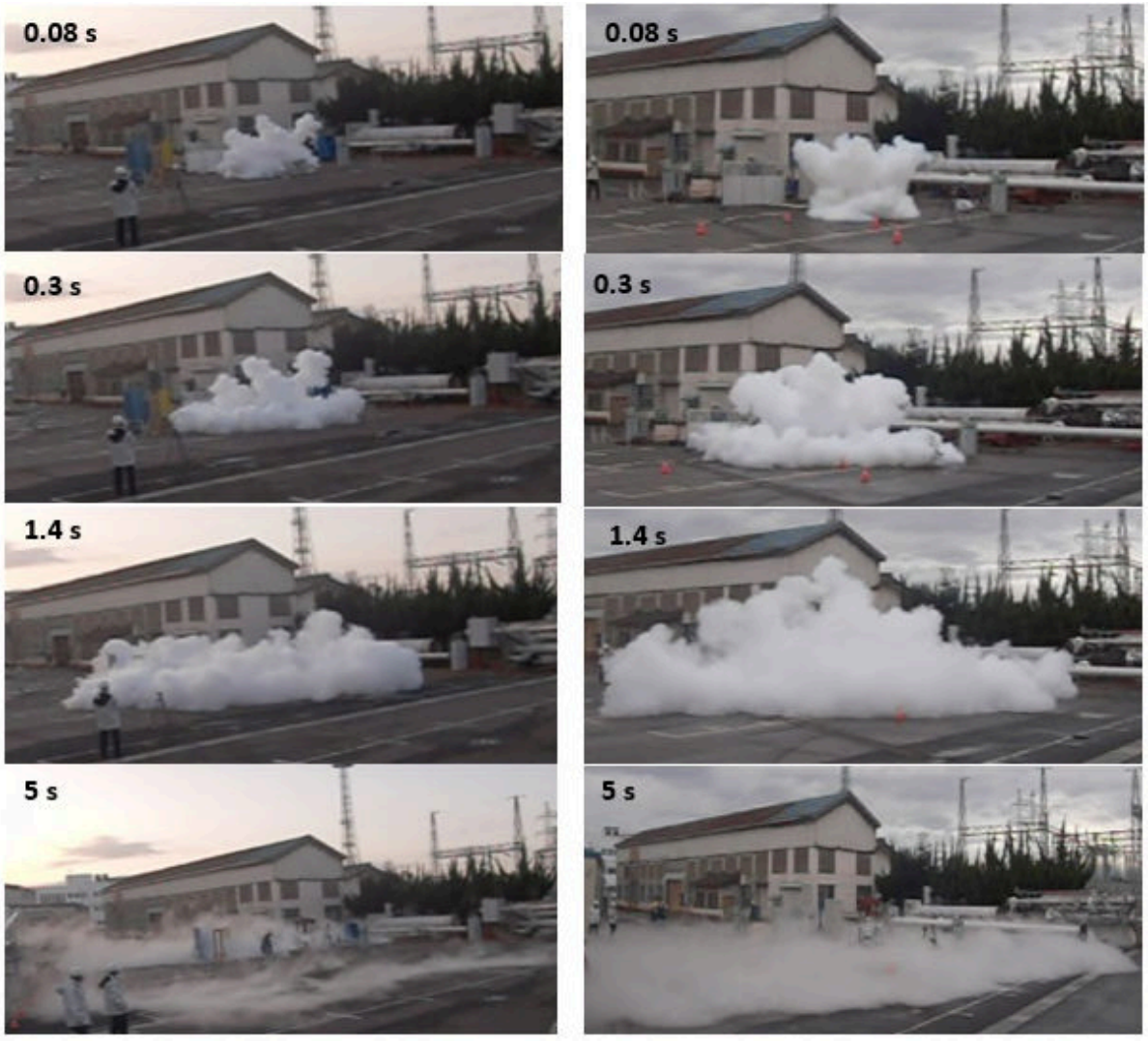

Fig. 21: Dispersion stage of the release in Test 1.2 (left) and Test 2.1 (right)

Table 4 Solid mass fraction generated during CO_2 expansion to atmospheric pressure as calculated through Equation 2 and 3; values for specific enthalpy obtained from NIST REFPROP V9.5 are adjusted to fit with the data given by Ekeberg, 2015 - which has another reference state

Test	Conditions	Specific enthalpy h_2 (kJ/kg)*	Solid enthalpy h_s (kJ/kg)*	Vapour enthalpy h_g (kJ/kg)*	Solid mass fraction (%)
Test 1.2	0.96 MPa, 231 K	330**	70.05	643.18	55
Test 2.1	1.65 MPa, 239 K	346.2**	70.05	643.18	51

*Under atmospheric pressure conditions
**specific enthalpy values are calculated thorough NIST REFPROPO V9.5 through input of initial pressure and temperature values and then adapted to the reference state

According to findings in Table 4, the theoretical thermodynamic reconstruction finds that solid mass fraction generating from the expansion of CO_2 at 0.96 MPa and (test 1.2) is 9% higher by mass than that the amount resulting from expansion of CO_2 at 1.65 MPa and (test 2.1). As previously presented in this study, the undertaken post-experimental qualitative observation suggested the presence of a larger amount of solid CO_2 accumulated inside and around the vessel after completion of test 1.2 compared to test 2.1 (shown in Fig. 9 and Fig. 19). It should be however emphasised that this approach is based on phenomena observation, and should be strengthened by quantitative analysis in future studies. In line with other empirical investigations (Koers, 2011; Ahmad et al., 2015; Sherpa Consulting, 2015) it is found that the released carbon dioxide expands in a characteristic 'tulip' shape (0.08 s), exhibiting the tendency to pool down on the ground in both test conditions (0.3 s) due to its density being higher than that of air as shown in Fig. 21. On the other hand, the jet undergoes an upwards-directed momentum, which is noticeably higher and longer-lasting at in test 2.1 and still clear at 1.4 s. In the first stage of the dispersion, the motion of the cloud is governed by inertia, and hence by its initial upstream conditions and atmospheric flow. As the cloud progressively moves away from the release point, air gets entrained, progressively reducing the concentration of carbon dioxide. The cloud then continues to propagate into a gravity spreading stage under the effect of buoyancy. Finally, as the cloud reaches a passive dispersion stage (5 s), a higher degree of mixing with air is enhanced by atmospheric turbulence, and its movement becomes solely subject to external ambient factors such as wind speed and direction (Sherpa Consulting, 2015).

4 Conclusions

This work investigated the real-scale discharge of liquid CO_2 from the emergency release coupler of marine loading arms to assess the impact on the surroundings and the facility, including the risk on personnel. Findings from this work are summarised in the following points:

- In all tests, the vertical separation of the coupler results in a violent radial leakage of the liquefied CO_2 inventory. The inventory fully discharges from the test vessel within 0-4 0.6 s of the start of the release.
- Carbon dioxide undergoes liquid – vapour – solid phase transitions whilst expanding to atmospheric pressure, with large clouds propagating during the dispersion stage; maximum depressurisation rates are hereby found to be considerably higher in medium pressure releases (1.62 – 1.65 MPa, test 2.1 and 2.2) compared to low pressure releases (0.87 – 0.96 MPa, test 1.1 and 1.2) implying a more violent discharge behaviour.
- Upon completion of discharges, the temperature inside the vessel achieved values of approximately 190 K in all tests. This implies the requirement for specific material selection for the emergency release coupler, given that the steel grades currently considered for liquid CO_2 shipping applications often exhibit minimum operating temperatures of 218 – 223 K.
- All tests are associated with the formation of a layer of carbon dioxide solids on the bottom and top surfaces of the test vessel; this requires further attention as it can disrupt the closure of the valves and disconnection of the coupler in real emergency shutdowns.
- The dispersion clouds surrounding the test vessel reach temperatures of 233 - 243 K within 0.1 – 0.27 s of the start discharge, implying an immediate risk for cryogenic impact to operators.
- Propagation of the jet assumes a characteristic ‘tulip’ shape that can be clearly observed from afar, with dispersion of the cloud taking approximately 5 s to dissipate.

Future work should focus on development of suitable models focusing on CO_2 discharge from emergency release systems, with the aim of enhancing the development of safety protocols as part of a risk assessment tool.

Acknowledgements

The authors would like to acknowledge Ministry of Environment of Japan for funding this project and the UKCCS Research Centre for funding international collaboration

References

Ahmad M, Lowesmith B, De Koeijer G, Nilsen S, Tonda H, Spinelli C, et al. COSHER joint industry project: Large scale pipeline rupture tests to study CO_2 release and dispersion. Int J Greenh Gas Control. 2015; 37:340–53.

Al Baroudi H, Awoyomi A, Patchigolla K, Jonnalagadda K, Anthony EJ. A review of large-scale CO_2 shipping and marine emissions management for carbon capture, utilisation and storage. Appl Energy 2021a;287:116510. https://doi.org/10.1016/j.apenergy.2021.116510.

Al Baroudi H, Patchigolla K, Thanganadar D, Jonnalagadda K. Experimental study of accidental leakage behaviour of liquid CO_2 under shipping conditions. Process Saf Environ Prot.2021b;pages 439-451. https://doi.org/10.1016/j.psep.2021.07.038

Bjerketvedt D, Egeberg K, Ke W, Gaathaug A, Vaagsaether K, Nilsen SH. Boiling liquid expanding vapour explosion in CO_2 small scale experiments. Energy Procedia 2011; 4:2285–92.

Brevik Engineering AS. (2020). CO2LOS II - Final Report with toolbox for CCS logistics. Available at: https://www.sintef.no/en/projects/2019/co2los-ii-co2-ship-transport-new-solutions/

Brown A, Eickhoff C, Reinders JEA, Raben I, Spruijt M, Neele F. IMPACTS: Framework for Risk Assessment of CO_2 Transport and Storage Infrastructure. Energy Procedia 2017;114:6501–13. https://doi.org/10.1016/j.egypro.2017.03.1786.

California State Lands Commission. Cabrillo Port Liquefied Natural Gas [LNG] Deepwater Port. 2006. Available at: https://ceqanet.opr.ca.gov/2004021107/3

Chiyoda Corporation. Preliminary Feasibility Study on CO_2 Carrier for Ship-based CCS（Phase-2 – unmanned offshore facility). Global CCS Institute. 2012. Available at: https://www.globalccsinstitute.com/resources/publications-reports-research/preliminary-feasibility-study-on-co2-carrier-for-ship-based-ccs-phase-2-unmanned-offshore-facility/

Ekeberg Danielsen, B. (2015). Investigation of Pressure Release Systems for CO_2. Norwegian University of Science and Technology.

Element Energy, Available at: 2018. TNO, Engineering Brevik, SINTEF, Polarkonsult.Shipping UK Cost Estimation Study. Available at: https://assets.publishing.service.gov.uk/government/uploads/system/uploads/attachment_data/file/761762/BEIS_Shipping_CO2.pdf

Energy Institute. Hazard analysis for offshore carbon capture platforms and offshore pipelines. 2013. Available at: https://www.globalccsinstitute.com/archive/hub/publications/115563/hazard-analysis-offshore-platforms-offshore-pipelines.pdf

Energy Institute. Technical guidance on hazard analysis for onshore carbon capture installations and onshore pipelines. 2010. Available at: https://www.globalccsinstitute.com/archive/hub/publications/7291/technical-guidance-hazard-analysis-onshore-carbon-capture-installations-and-onshore-pipelines.pdf

Guo X, Yan X, Yu J, Yang Y, Zhang Y, Chen S, et al. Pressure responses and phase transitions during the release of high-pressure CO_2 from a large-scale pipeline. Energy. 2017; 118:1066–78.

Han SH, Chang D. Dispersion analysis of a massive CO_2 release from a CO_2 carrier. Int J Greenh Gas Control 2014; 21:72–81.

Han SH, Chang D, Kim J, Chang W. Experimental investigation of the flow characteristics of jettisoning in a CO_2 carrier. Process Saf Environ Prot. 2014;92[1]:60–9.

Harper P, Wilday J, Bilio M. Assessment of the major hazard potential of carbon dioxide. 2015; Health and Safety Executive.

Holt, H., Helle, K., & Brown, J. (2012). CCS CO_2 risk management - new industry guidance. Institution of Chemical Engineers Symposium Series, 158, 133–141.

Huh C, Kang S, Park M, Lee K, Park Y, Min D, et al. Latest CO_2 Transport, Storage and Monitoring R&D Progress in Republic of Korea: Offshore Geologic Storage. Energy Procedia. 2013; 37:6520–6.

IEAGHG. The Status and Challenges of CO_2 Shipping Infrastructures. 2020; IEAGHG Technical Report 2020-10.

Jakobsen J, Roussanaly S, Anantharaman R. A techno-economic case study of CO_2 capture, transport and storage chain from a cement plant in Norway. J Clean Prod. 2017; 144:523–39.

Koers P, Maarten de Looij. Safety Study for Liquid Logistics Shipping Concept. 2011;. Rotterdam, Det Norske Veritas BV. Report number: 12TUIBY-3

Li K, Zhou X, Tu R, Yi J, Xie Q, Jiang X. Experimental Investigation of CO_2 Accidental Release from a Pressurised Pipeline. Energy Procedia. 2015; 75:2221–6.

Li M, Liu Z, Zhou Y, Zhao Y, Li X, Zhang D. A small-scale experimental study on the initial burst and the heterogeneous evolution process before CO_2 BLEVE. J Hazard Mater. 2018; 342:634–42.

Luketa, A., & Hightower, M. (2018). Guidance on Hazard and Safety Analyses of LPG Spills on Water. Sandia National Laboratories Report

Ministry of Petroleum and Energy Norway, Gassco, Gassnova. Feasibility study for full-scale CCS in Norway. 2016. Available at: https://ccsnorway.com/wp-content/uploads/sites/6/2019/09/feasibilitystudy_fullscale_ccs_norway_2016.pdf

Mitsubishi Heavy Industries. Report on Ship Transport of CO_2. 2004; IEA Greenhouse Gas R&D Programme. https://ieaghg.org/docs/General_Docs/Reports/PH4-30%20Ship%20Transport.pdf

Noh H, Kang K, Huh C, Kang SG, Seo Y. Identification of potential hazardous events of unloading system and CO_2 storage tanks of an intermediate storage terminal for the Korea clean carbon storage project 2025. Int J Saf Secur Eng. 2018;8[2]:258–65.

Ozaki M, Ohsumi T, Kajiyama R. Ship-based offshore CCS featuring CO_2 shuttle ships equipped with injection facilities. Energy Procedia 2013;37:3184–90. https://doi.org/10.1016/j.egypro.2013.06.205.

Pitblado R, Baik J, Hughes GJ, Ferro C, Shaw SJ. Consequences of LNG Marine

Incidents. Det Norske Veritas (USA) Inc. CCPS Conference Orlando. 2004

Pursell M. Experimental investigation of high-pressure liquid CO_2 release behaviour. Inst Chem Eng Symp Ser. 2012;[158]:164–71.

Seo Y, Huh C, Lee S, Chang D. Comparison of CO_2 liquefaction pressures for ship-based carbon capture and storage [CCS] chain. Int J Greenh Gas Control. 2016; 52:1–12.

Shafiq U, Shariff AM, Babar M, Ali A. A study on blowdown of pressurized vessel containing CO_2 /N_2/H_2S at cryogenic conditions. IOP Conf Ser Mater Sci Eng. 2018;458[1].

Sherpa Consulting. Dispersion modelling techniques for carbon dioxide pipelines in Australia. Global CCS Institute. 2015. Available at: https://www.globalccsinstitute.com/archive/hub/publications/196358/dispersion-modelling-techniques-carbon-dioxide-pipelines-australia.pdf

SIGTTO. Liquefied Gas Handling Principles On Ship and in Terminals, 4TH edition. Witherby Seamanship. ISBN: 9781856097147. 2016

SIGTTO. LNG Emergency Release Systems - Recommendations, Guidelines and Best Practices. Witherby Seamanship; 2017. ISBN: 9781856097307

Skagestad R, Eldrup N, Richard H, Belfroid S, Mathisen A, Lach A, Haugen HA. Ship transport of CO_2 - Status and Technology Gaps. Tel-Tek. 2014.

Teng L, Li Y, Zhao Q, Wang W, Hu Q, Ye X, et al. Decompression characteristics of CO_2 pipelines following rupture. J Nat Gas Sci Eng. 2016; 36:213–23.

Tokyo Boeki Engineering. Marine Loading Arms (brochure). Available at: http://www.tokyo-boeki-eng.co.jp/technology/pdf/marine%20loading%20arms_E.pdf

Tosse S, Vaagsaether K, Bjerketvedt D. An experimental investigation of rapid boiling of CO_2. Shock Waves 2015;25:277–82. https://doi.org/10.1007/s00193-014-0523-6.

Van der Voort MM, van Wees RMM, Ham JM, Spruijt MPN, van den Berg AC, de Bruijn PCJ, et al. An experimental study on the temperature dependence of CO_2

explosive evaporation. J Loss Prev Process Ind 2013; 26:830–8.

Vermeulen TN. Knowledge sharing report – CO_2 Liquid Logistics Shipping Concept [LLSC]: Overall Supply Chain Optimization 2011:143. Available at: https://www.globalccsinstitute.com/resources/publications-reports-research/knowledge-sharing-report-co2-liquid-logistics-shipping-concept-business-model/

Wang C, Li Y, Teng L, Gu S, Hu Q, Zhang D, et al. Experimental study on dispersion behavior during the leakage of high-pressure CO_2 pipelines. Exp Therm Fluid Sci. 2019; 105:77–84.

Worley Parsons, Schlumberger, McKenzie B&, EPRI. Strategic Analysis of the Global Status of Carbon Capture and Storage - Report 1: Status of Carbon Capture and Storage Projects Globally. Global CCS Institute. 2009. Available at: https://www.globalccsinstitute.com/archive/hub/publications/5751/report-5-synthesis-report.pdf

Worley Parsons. CCS learning from the LNG sector - A report for the Global CCS Institute. 2013.

Xie Q, Tu R, Jiang X, Li K, Zhou X. The leakage behavior of supercritical CO_2 flow in an experimental pipeline system. Appl Energy. 2014; 130:574–80.

Yangle W, Yuan Z, Yanping H, Jingtan C, Junfeng W. Modelling of accidental release process from small rupture of pressure CO_2 vessel. Int J Greenh Gas Control. 2020; 93:1–10.

Yoo BY, Choi DK, Kim HJ, Moon YS, Na HS, Lee SG. Development of CO_2 terminal and CO_2 carrier for future commercialized CCS market. Int J Greenh Gas Control. 2013; 12:323–32.

Zahid U, An J, Lee C, Lee U, Han C. Design and Operation Strategy of CO_2 Terminal. Ind Eng Chem Res. 2015;54[8]:2353–65.

ZEP. Role of CCUS in a below 2 degrees scenario 2018:1–30. https://zeroemissionsplatform.eu/wp-content/uploads/ZEP-Role-of-CCUS-in-below-2c-report.pdf

Zheng W, Mahgerefteh H, Martynov S, Brown S. Modeling of CO_2 Decompression across the Triple Point. Ind Eng Chem Res. 2017;56[37]:10491–9.

Zhou X, Li K, Tu R, Yi J, Xie Q, Jiang X. Numerical Investigation of the Leakage Flow from a Pressurized CO_2 Pipeline. Energy Procedia. 2014; 61:151–4.